Direct Imaging of Temperature-Dependent Layered Antiferromagnetism of a Magnetic Oxide

M. Konoto,[1] T. Kohashi,[2] K. Koike,[3,4] T. Arima,[1,5] Y. Kaneko,[1] T. Kimura,[6,*] and Y. Tokura[1,4,6]

[1]*Spin Superstructure Project, ERATO, Japan Science and Technology Agency (JST), Tsukuba 305-8562, Japan*
[2]*Hitachi, Ltd., Central Research Laboratory, Kokubunji 185-8601, Japan*
[3]*Graduate School of Science, Hokkaido University, Sapporo 060-0810, Japan*
[4]*Correlated Electron Research Center (CERC), National Institute of Advanced Industrial Science and Technology (AIST), Tsukuba 305-8562, Japan*
[5]*Institute of Materials Science, University of Tsukuba, Tsukuba 305-8573, Japan*
[6]*Department of Applied Physics, University of Tokyo, Tokyo 113-8656, Japan*
(Received 29 December 2003; published 2 September 2004)

With the use of a newly developed spin-polarized scanning electron microscope, we have succeeded in obtaining the real-space images of the layered-antiferromagnetic state concurrent with 1-nm-stepped atomic terraces in layered-structure manganite $La_{1.4}Sr_{1.6}Mn_2O_7$. The three-dimensional analysis of spin alignment could further reveal the temperature-dependent spin reorientation and the antiferromagnetic domain walls on the atomic terraces. These ensure the use of the present microscopy for quantitative analysis of local magnetic structures in a broader range of materials, including magnetic oxides and nanomaterials.

Rapid progress of spintronics in past years is increasing the importance of magnetically sensitive microscopy with nanometer resolution. Since the local spin arrangement plays a determining role in physical basis, further development of local probing technique of spin alignment is crucial for establishing a fundamental principle and realizing practical devices. During this decade, spin-polarized scanning electron microscopy (spin SEM or SEMPA) [1], X-ray photoemission electron microscopy [2], and spin-polarized low energy electron microscopy [3] have made great progress, with the lateral resolution approaching the sub-10 nm range. Among them, spin SEM can give the clear understanding for domain structures characteristic of a surface [4] as well as for micromagnetic structures in ultrathin films [5] and multilayers [6], fully exploiting the extremely small probing depth [7] and the quantitative analysis of magnetization orientation [8]. Recently, we have developed a spin SEM type instrument equipped with a low temperature sample stage integrated with *in situ* cleavage system. This instrument can probe three magnetization-vector components simultaneously at high resolution [9,10]. Up to now, Allenspach and co-workers have applied a similar technique to metallic ultrathin films at the temperature ranging from 90 K to room temperature and successfully obtained the images of domain evolution [11]. Our main subject is the magnetism of perovskite manganites and related materials, which are promising for spintronics as will be mentioned below. In spite of their attractive properties, there have been only a few microscopic studies based on the analysis of magnetization orientation, since cryogenic measurement is required in most cases [12]. Our sample stage has the ability to control sample temperature within the range from around 30 to 800 K, which enables us to scrutinize local magnetization arrangement of various kinds of materials including perovskite manganites [13]. In addition, the function of *in situ* cleavage under ultra-high vacuum is especially effective in yielding a clean surface for cleavable crystals like the manganites.

Perovskite manganites and their family exhibit novel characteristics suitable for spintronic materials, such as a high degree of spin polarization [14,15] and colossal magnetoresistance [16–18]. Especially, a layered-structure compound $La_{1.4}Sr_{1.6}Mn_2O_7$ has been attracting enormous interest because of its remarkably large interlayer tunneling magnetoresistance up to 4000%, which results from the layered antiferromagnetism (AF) state [18,19]. Because the crystal includes ferromagnetic portions due to the tendency of phase coexistence inherent to the layered manganites, the magnetic structure postulated by neutron diffraction technique is still less clear [20,21]. Therefore, a phase-selective measurement based on a local probing technique is indispensable for confirming the magnetic structure of each phase. The direct observation of the antiferromagnetic phase has, however, been pending for a long time due to technical difficulty. As for the local magnetic probe with high spatial resolution, spin STM has been successfully applied to observation of the layered AF of an atomically stepped Cr (001) surface at room temperature [22] by making use of an -exchange-split surface state [23]. Since the variable-temperature spin SEM can obtain a magnetic image without use of such a special surface state, as well as with its excellent characteristics mentioned above, it is anticipated to provide a powerful technique for the study of the local magnetic structure, including such a layered AF state, of the magnetic oxides. Moreover, the variable-temperature observation can provide the temperature dependence of both in-plane and out-of-plane angles of

magnetization and its spatial distribution which are critical issues for the study of spintronics.

The variable-temperature spin SEM is composed of an electron gun with Schottky-type field emitter [24], an electron transfer optical system optimized by numerical simulation [9], a Mott type spin detector equipped with a spin rotator, a variable-temperature sample stage, and an image acquisition system. The three magnetization-vector components, M_x, M_y, and M_z, can be obtained by the combination of the spin rotator and spin detector [10]. M_x and M_y are detected by switching off the rotator, while M_z by switching on the rotator. This off-and-on sequence is made for each pixel, which enables quasisimultaneous detection of the three magnetization-vector components. The specially designed sample stage is equipped with the temperature control and crystal cleavage system under ultra high vacuum [25].

A single crystal of $La_{1.4}Sr_{1.6}Mn_2O_7$ was prepared using a floating zone method as previously described [17]. The crystal was cooled to about 40 K on the sample stage in the spin SEM observation chamber with the base pressure of 3×10^{-10} Torr, and then cleaved to produce a clean ab surface plane. After stabilizing the temperature, images of topography and three magnetization-vector components, M_x, M_y, and M_z, at the cleaved surface plane were obtained simultaneously in a remanent state. Here M_x and M_y are parallel to the cleaved plane and made right angle to each other, and M_z is perpendicular to the plane.

The crystallographic and magnetic structures of $La_{1.4}Sr_{1.6}Mn_2O_7$ are schematically shown in Fig. 1. The basic crystallographic structure is the alternate stacking of a nonmagnetic insulating $(La, Sr)_2O_2$ layer and a ferromagnetic metallic MnO_2 bilayer sheet along the c axis [18]. The magnetic structure of the antiferromagnetic

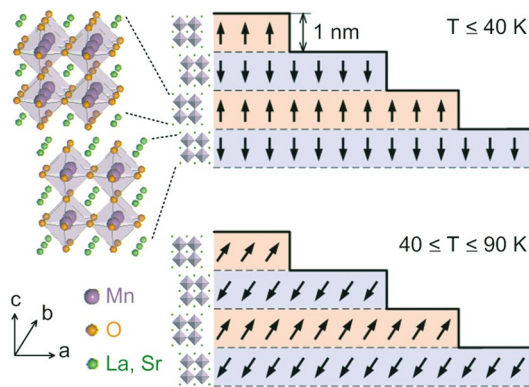phase presented here was postulated by former neutron diffraction experiments [20,21]. The coupling of magnetization is ferromagnetic within the constituent MnO_2 bilayer and weakly antiferromagnetic between the adjacent bilayers, leading to the layered AF. The magnetization aligns along the c axis at low temperatures as illustrated in the top drawing. As the temperature is increased, the magnetization inclines toward the ab plane and eventually vanishes at about 90 K [18]. Therefore, alternating spin arrangement can be anticipated at the surface terraces separated by half-unit-cell ($c/2 = 1$ nm) steps, reflecting the layered AF.

Figure 2 shows (a) topographic and (b) magnetic images on the cleaved ab plane observed simultaneously at 60 K. The magnetic image is obtained from the in-plane magnetization component parallel to the arrows. Faintly visible white lines in the topographic image, only some of which are indicated by arrows in Fig. 2(a), are considered to be step edges, where the secondary electron yield is enhanced due to the edge effect [26]. The observed contrast enhancement of only 1% is detected using pulse-count-type electron counters installed in the spin detector [27]. The acquisition time is 60 min, long enough to reduce the statistical errors in pulse counting. The locations of those lines exactly coincide with the distinct boundaries of magnetic contrast in Fig. 2(b). In order to determine the step height on the cleaved plane, surface topography was measured with an atomic force microscope (AFM). Figure 2(c) indicates a typical plane view image of the cleaved surface [a different region from Fig. 2(a)]. There are five flat terraces in this image. The height profile along the white line is also shown (bottom drawing). The step height of 1 nm is entirely consistent with the thickness ($= c/2$) of the stacking unit of the layered AF. In the other regions scrutinized by the AFM, essentially the same structures as shown in Fig. 2(c) are commonly observed, that is step and terrace structure

FIG. 1 (color). Schematic diagram of the layered crystallographic and antiferromagnetic structures of $La_{1.4}Sr_{1.6}Mn_2O_7$. MnO_6 octahedra are shown in polyhedral representation. Indicated magnetic structures were postulated by neutron diffraction studies [20,21]. Ferromagnetically coupled spins within the MnO_2 bilayers are distinguished with different colors.
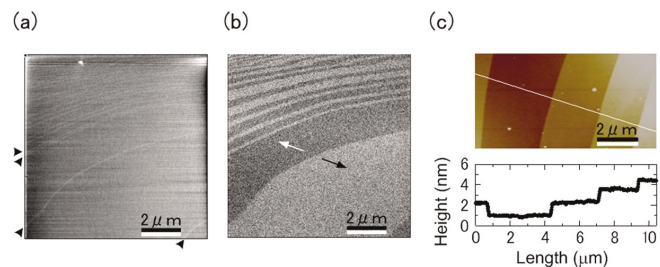

FIG. 2 (color). (a) Topographic and (b) magnetic images observed simultaneously with the spin-polarized scanning electron microscopy (spin SEM) for the same area of the cleaved ab plane of $La_{1.4}Sr_{1.6}Mn_2O_7$ at 60 K. The magnetic contrast image is obtained using the in-plane magnetization component parallel to the arrows. (c) Topographic image of the cleaved plane [a different region from that shown in (a) and (b)] and the height profile along the white line measured with an atomic force microscope (AFM).

with the step height of 1 nm. These results strongly indicate that the single crystal is cleaved along $(La, Sr)_2O_2$ insulating layers with sodium chloride structure, yielding several micrometers broad terraces of MnO_2 bilayers. Note that the spin-sensitive probing depth of the spin SEM is estimated to be about 1 nm [7]. These facts ensure that the present spin SEM observation provides the direct imaging of the layered AF structure. We have also observed local regions with a ferromagnetic structure incorporated with the layered AF region. The ferromagnetic local region exhibited a different temperature dependence of magnetism. We will discuss the tendency of the phase coexistence inherent to this layered manganite elsewhere and here focus on the magnetic structure of the layered AF.

The temperature dependence of the respective magnetization components, M_x, M_y, and M_z, is displayed in Fig. 3(a). The red broken lines denote the location of step edges appearing in the topographic image (not shown) of the same area. The blue broken line, where no topographic contrast is observed, is considered to be an AF domain wall lying on the atomically flat terrace as

discussed below. At 50 K, the magnetization is almost parallel to the c axis: M_z is much larger than M_x and M_y. The quantitative structure is shown by the color image at the bottom of Fig. 3(b). Here the color shows the out-of-plane magnetization direction, and the relationship between the color and the direction is given by the color wheel at the top of Fig. 3(b). The cross-sectional view of magnetization direction along the white line is also given schematically at the middle of Fig. 3(b). Along this line, the atomic terrace being left to the step is colored blue where the magnetization points upper right. The out-of-plane angle is estimated to be about 75° to the ab plane. In the middle part of the terrace, the magnetization points precisely in the opposite direction as represented by greenish yellow, namely, lower left. Across the vertical blue broken line, only the perpendicular component M_z changes its sign, while no step is observed in the topographic image. Thus, we could assign this to the AF domain wall on the same atomically flat terrace. This change of magnetization direction across the AF domain boundary makes striking contrast to that at the step edge where *all* the **M** vector components change their signs.

The temperature-dependent variation of the magnetization direction on each region is directly observed. M_z obviously decreases with an increase in temperature to 60 K, while M_x and M_y slightly increase. The result shows that the magnetization gradually inclines toward the ab plane. No particular change in the position is detected at the step (the red broken line in Fig. 3) during the heating, whereas the boundary represented by the blue broken line considerably changes in shape and position. The deformation of the boundary associated with the change only in M_z also ensures that this boundary is the AF domain wall on the same flat atomic terrace of the bilayer. At 70 K, since M_z almost vanishes, the magnetization becomes
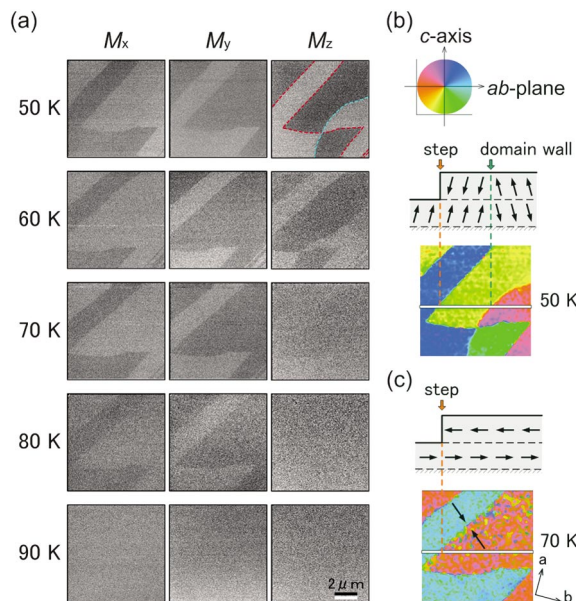

FIG. 3 (color). (a) Temperature dependence of the in-surface-plane magnetization components, M_x and M_y, and the surface-normal component, M_z, at the cleaved surface of the $La_{1.4}Sr_{1.6}Mn_2O_7$ crystal. The red broken lines in the 50 K M_z image denote the location of the step edges assigned by the topographic image. Color images at the bottom of (b) and (c) are obtained by the out-of-plane magnetization direction at 50 and 70 K, respectively. The relationship between the color and the out-of-plane direction is represented by the color wheel at the top of (b). The schematic cross-section views of the magnetization direction along the white lines are shown at the middle of (b) and at the top of (c). The crystallographic orientation determined by Laue diffraction is indicated at the right side of (c).
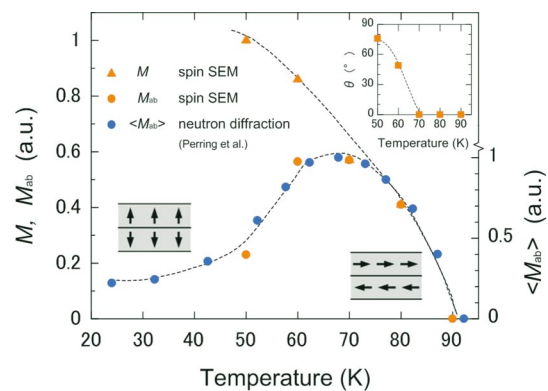

FIG. 4 (color). Temperature dependence of the total magnetization M (red triangles) and the in-plane component M_{ab} (red circles) of $La_{1.4}Sr_{1.6}Mn_2O_7$ as deduced by the spin SEM observation. The angle between magnetization and the ab plane θ is indicated in the inset. For comparison, the in-plane magnetization component $\langle M_{ab} \rangle$ (blue circles) estimated by the neutron diffraction study [20] is also shown.

nearly parallel to the *ab* plane. The arrows in the image at the bottom of Fig. 3(c) show the magnetization directions in the *ab* plane. Magnetization in each region, which is separated by the step edge, directs opposite to each other in the *ab* plane as represented by red and light blue colored regions, and makes an angle of about 45° off the *a* or *b* direction as shown by the arrows at the right side of the image. The in-plane magnetization component always keeps the same direction throughout the heating process. The magnitude of these components gradually decreases as the temperature increases, and finally disappears at 90 K, reflecting the transition to a paramagnetic state.

Figure 4 depicts the temperature dependence of the magnetization M and its in-plane component M_{ab} calculated from the respective magnetization components shown in Fig. 3(a). The total magnetization is given by $M = \sqrt{M_x^2 + M_y^2 + M_z^2}$. The in-plane component is given by $M_{ab} = M\cos\theta$, where $\theta = \tan^{-1}(M_z/\sqrt{M_x^2 + M_y^2})$ denotes the angle between the magnetization vector and the *ab* plane. The temperature dependence of θ is shown in the inset. For comparison, the in-plane magnetization component $\langle M_{ab}\rangle$ which was estimated from the neutron diffraction measurement by Perring *et al.* [20] is also shown. This component can be obtained as the square root of the diffraction intensity for the (005) peak probing the in-plane antiferromagnetic long-range order. As can be seen, M monotonically decreases with increase in temperature and vanishes at 90 K, namely, the magnetic transition temperature [18]. In contrast, M_{ab} gradually increases and reaches a maximum at around 70 K where the perpendicular component fades away as illustrated in Fig. 3. The increase in M_{ab} with the temperature up to 70 K demonstrates that the magnetization gradually inclines toward the *ab* plane. The decrease in M_{ab} above 70 K reflects the reduction of the total magnetization. The in-plane magnetization component $\langle M_{ab}\rangle$ obtained from the neutron diffraction markedly increases with the temperature change from 40 to 70 K and reaches a maximum at 70 K. Above 70 K, $\langle M_{ab}\rangle$ decreases and vanishes away at around 90 K [28]. The essential agreement between the present real-space observation and the result of the neutron diffraction by Perring *et al.* [20] indicates that the spatial distribution of spin arrangement of $La_{1.4}Sr_{1.6}Mn_2O_7$ could be directly and excellently probed using the present variable-temperature spin SEM. The layered AF arrangement and the temperature-dependent spin reorientation have thus been directly confirmed by the present local probing technique. Moreover, we have provided the in-plane and out-of-plane angles of the magnetization in the layered AF phase. The present microscopy can provide a spatially resolved probe for the spin arrangement at the surface of various magnetic oxides and related materials.

*Present address: Los Alamos National Laboratory, Los Alamos, NM 87545, USA.

[1] R. Frömter, H. P. Oepen, and J. Kirschner, Appl. Phys. A **76**, 869 (2003).

[2] W. Swiech *et al.*, J. Electron Spectrosc. Relat. Phenom., **84**, 171 (1997); S. Anders *et al.*, Rev. Sci. Instrum. **70**, 3973 (1999).

[3] T. Duden and E. Bauer, Rev. Sci. Instrum. **66**, 2861 (1995); E. D. Tober, G. Witte, and H. Poppa, J. Vac. Sci. Technol. A **18**, 1845 (2000).

[4] J. Unguris *et al.*, Appl. Phys. Lett. **55**, 2553 (1989); K. Koike *et al.*, Appl. Phys. Lett. **62**, 2581 (1993).

[5] R. Allenspach, M. Stampanoni, and A. Bischof, Phys. Rev. Lett. **65**, 3344 (1990); H. P. Oepen, J. Magn. Magn. Mater. **93**, 116 (1991).

[6] J. A. Borchers *et al.*, Phys. Rev. Lett. **82**, 2796 (1999).

[7] D. L. Abraham and H. Hopster, Phys. Rev. Lett. **58**, 1352 (1987).

[8] G. G. Hembree *et al.*, Scanning Microsc. Suppl. **1**, 229 (1987).

[9] T. Kohashi and K. Koike, Jpn. J. Appl. Phys. **40**, L1264 (2001).

[10] T. Kohashi, M. Konoto, and K. Koike, Rev. Sci. Instrum.. (to be published).

[11] R. Allenspach, J. Magn. Magn. Mater. **129**, 160 (1994).

[12] A. Gupta *et al.*, Phys. Rev. B **54**, 15629(R) (1996).

[13] M. Konoto *et al.*, Appl. Phys. Lett. **84**, 2361 (2004).

[14] C. Zener, Phys. Rev. **82**, 403 (1951).

[15] J.–H. Park *et al.*, Nature (London) **392**, 794 (1998).

[16] R. von Helmolt *et al.*, Phys. Rev. Lett. **71**, 2331 (1993).

[17] Y. Moritomo *et al.*, Nature (London) **380**, 141 (1996).

[18] T. Kimura *et al.*, Science **274**, 1698 (1996).

[19] T. Kimura *et al.*, Phys. Rev. Lett. **79**, 3720 (1997).

[20] T. G. Perring *et al.*, Phys. Rev. B **58**, 14693(R) (1998).

[21] D. N. Argyriou *et al.*, Phys. Rev. B **59**, 8695 (1999).

[22] M. Kleiber *et al.*, Phys. Rev. Lett. **85**, 4606 (2000); T. Kawagoe *et al.*, J. Appl. Phys. **93**, 6575 (2003).

[23] J. A. Stroscio *et al.*, Phys. Rev. Lett. **75**, 2960 (1995).

[24] D. W. Tuggle and L. W. Swanson, J. Vac. Sci. Technol. B **3**, 220 (1985).

[25] M. Konoto, T. Kohashi, and K. Koike (unpublished).

[26] H. Seiler, J. Appl. Phys. **54**, R1 (1983).

[27] It has been reported that contrast enhancement at the atomic layer steps whose height is smaller than the spatial resolution could be detected with a scintillation counter. For example, see K. Kuroda *et al.*, Scanning Microsc. **1**, 911 (1987).

[28] The inclination angle has been estimated by Argyriou *et al.* (Ref. [21]), from the diffraction intensities of the crystal with coexisting two magnetic phases. The estimated angle is, however, not consistent with the present result.